frontiers | Frontiers in Nanotechnology

TYPE Original Research
PUBLISHED 24 March 2025
DOI 10.3389/fnano.2025.1477247

OPEN ACCESS

EDITED BY
Sandeep Kumar,
Punjab engineering college (Deemed to be University), India

REVIEWED BY
Jia-Cheng E. Yang,
Chinese Academy of Sciences (CAS), China
Ramacharyulu P. V. R. K,
Pukyong National University, Republic of Korea
Sharf Ilahi Siddiqui,
University of Delhi, India

*CORRESPONDENCE
Ramesh Namdeo Pudake,
rnpudake@amity.edu
Sandip Chakrabarti,
schakrabarti@amity.edu

RECEIVED 07 August 2024
ACCEPTED 12 March 2025
PUBLISHED 24 March 2025

CITATION
Bhattacharyya P, Pudake RN and Chakrabarti S (2025) A silver functionalized ZIF-8 derived heterostructure with excellent visible-light-driven photocatalytic removal of antibiotics. *Front. Nanotechnol.* 7:1477247. doi: 10.3389/fnano.2025.1477247

A silver functionalized ZIF-8 derived heterostructure with excellent visible-light-driven photocatalytic removal of antibiotics

Puja Bhattacharyya[1], Ramesh Namdeo Pudake[1]* and Sandip Chakrabarti[2]*

[1]Amity Institute of Nanotechnology, Amity University Uttar Pradesh, Noida, India, [2]Amity Institute of Click Chemistry Research and Studies, Amity University Uttar Pradesh, Noida, India

An effective silver (Ag) -modified zeolitic imidazolate frameworks- ZIF-8 derived heterostructure (Ag/ZnO/C) was prepared using the facile room temperature wet chemical method for the reduction of Ciprofloxacin under visible light irradiation. The synthesized Ag/ZnO/C microstructure was characterized by field emission scanning electron microscopy (FESEM) and transmission electron microscopy (TEM) analysis. X-ray diffraction (XRD), X-ray photoelectron spectroscopy (XPS), and TEM morphological analysis confirmed the existence of metallic Ag in the resultant photocatalyst. The synergistic effect of the Metal–organic frameworks (MOF) - derived structure and metallic Ag nanoparticles depicts excellent degradation of Ciprofloxacin with high efficiency. Under optimum condition the efficiency was reached to 98% in 60 min under visible light irradiation. The apparent rate constant k is estimated as 58.04×10^{-3} min^{-1} depicting high photocatalytic performance. The scavenger experiment revealed the dominance of generated h^+ and $\cdot O_2^-$ in the photocatalysis mechanism. The large surface area and successful silver nanoparticle encapsulation on the material surface facilitates to the excellent efficiency of the material. Our findings open new robust possibilities to design a ZIF-8 based efficient photocatalyst for effective application in the field of photo-degradation.

KEYWORDS

photocatalysis, metal-organic frameworks, antibiotics, porous nanostructure, silver

1 Introduction

The release of pollutants from various industries into the water sources creates a significant environmental concern. Effective treatment of these pollutants in water is necessary for achieving safe drinking water. Recent approaches like ion exchange, flocculation, photocatalytic degradation, coagulation, biodegradation, electrolysis, chemical oxidation, precipitation, and adsorption, have been conventionally adopted (Oh et al., 2024). But, among them, photocatalytic degradation is considered as an eco-friendly solution for efficient water purification (Chen et al., 2024). Antibiotics are a special class of medications employed for human health, animal care, and agricultural applications, and a dramatic increase in their use and discharge has been reported globally (Gangar and Patra, 2023). The problem of environmental contamination has sparked widespread terror

in many nations. One of the main sources of water pollution that harms people's health incalculably is wastewater containing antibiotics (Bhattacharyya et al., 2021; Mishra et al., 2023). A popular class of synthetic antibiotics known as fluoroquinolones is frequently used to treat infectious infections in both people and animals (Assar et al., 2021). Ciprofloxacin (CIP) is the fluoroquinolone that is most frequently prescribed worldwide for urinary tract infections, sexually transmitted infections, skin, bone, joint infections, prostatitis, typhoid fever, gastrointestinal infections, lower respiratory tract infections, anthrax, plague, and salmonellosis (Shariati et al., 2022). The excretion of unmodified CIP and their metabolites in household wastewater results from both regular medications and the illicit use of these antibiotics (Bhatt and Chatterjee, 2022). Due to this its concentration in water bodies has grown over time. It needs to be eliminated from wastewater as it negatively impacts both human health and the health of other creatures in the aquatic ecosystem (Hayri-Senel et al., 2024; Ahmad et al., 2024). One of the environmentally friendly processes that can successfully decompose organic molecules using unrestricted solar energy is visible-light-driven photocatalysis (Hussain et al., 2021; Fatima et al., 2019). Efforts have been made to optimize semiconductor photocatalysts with increased activity and stability to increase the photocatalytic efficiency when exposed to visible light. A novel class of porous material consisting of metal ions and organic compounds is called a metal-organic framework (MOF), and has been widely used in gas storage, separation, photocatalysis, and drug administration due to its permanent nano-scale porosity, consistent structural cavity, extraordinarily high surface area, superior thermal stability, and mechanical stability (Pettinari et al., 2017; Basak et al., 2024). In addition, moderate pyrolysis of MOF yields carbon-based metal oxides with excellent porous structures possessing surprising adsorption or catalytic capabilities (Wang C. et al., 2020). The regular and accessible porous structure of pristine MOF and its pyrolysis derivative were suitable matrices for incorporating functional nanoparticles (Xiao et al., 2023).

Zeolitic imidazolate frameworks (ZIFs) are porous hybrid materials that have zeolite-like structures and are constructed from four connected nets of tetrahedral units. Metal ions, such as Zn^{2+} or Co^{2+}, are linked through N atoms in diatopic imidazolate anions (Liu et al., 2021). Moreover, ZIF structures are associated with the advantages of zeolites and MOFs including properties like high porosity, crystallinity, and excellent thermal and chemical stability. One of the most extensively researched ZIF materials at the moment for a variety of applications is ZIF-8 (Dai et al., 2021; Li et al., 2024) ZIF-8 or Zn (mIm)2 (where mIm is the 2-methyl imidazolate) possess a solid topology featuring an I-43 space group with a pore width and accessible diameter of 11.6 Å and 3.4 Å, respectively. The structure of ZIF-8 and its derivatives is quite stable which allows for long-term application, Numerous experts have carried out more research on it because of its robustness and versatile application (Bergaoui et al., 2021).

The photocatalytic degradation of environmental contaminants using semiconductor photocatalysts has gained increased attention in recent years. Recent research findings show that porous MOFs are a possible new class of photocatalysts for their ability to degrade organic pollutants through catalysis. The photoactive MOFs offer several benefits over traditional semiconductor photocatalysts when it comes to decomposing organic contaminants (Hussain et al., 2021). The well-defined crystalline structures of MOFs have tailorable electronic structures with tunable active sites leading to more efficiency of solar harnessing. MOFs are distinguished from traditional inorganic semiconductors by having molecules organized in a crystalline lattice rather than a delocalized conduction band (CB) and valence band (VB). Because MOFs can select from a wide range of metal ions/clusters and organic linkers, they are highly adjustable photocatalysts that can efficiently use solar light (Wang Q. et al., 2020). Moreover, the incorporation of Ag nanoparticles into the nanostructures can further promote the separation efficiency of photo-induced carriers thus elevating the overall photocatalytic activity (Elhalil et al., 2019; Tran et al., 2019).

In this study, we used the well-known MOF structure ZIF-8 as a template to create ZnO nanostructure through high-temperature pyrolysis (Wang et al., 2019), which was then used as the porous host for silver (Ag^0) nanoparticles. A promising heterostructure was designed by incorporating Ag nanoparticles into porous ZnO which derived from the pyrolysis of ZIF-8 for visible light-driven photocatalysis. A room-temperature wet chemical method was used for the synthesis of the Ag/ZnO heterostructure. The synthesized heterojunction displayed outstanding catalytic activity and a high catalytic efficiency against the popular antibiotic ciprofloxacin under the influence of visible light.

2 Experimental materials and method

2.1 Materials

Zinc nitrate ($Zn(NO_3)_2$, ≥98%), ZnO (>97%), 2-methylimidazole (≥99%), silver nitrate ($AgNO_3$, ≥99.99%), sodium borohydride ($NaBH_4$, ≥ 99%) and CIP (≥98%) were purchased from Sigma Aldrich, United States. The solvent methanol (≥99.9%), was purchased from Qualigens, United States. All chemicals and reagents were of analytical grade and used without further purification.

2.2 Synthesis of ZIF-8 and porous ZnO nanostructures

ZIF-8, a metal-organic framework, was synthesized by room temperature precipitation method. Typically, $Zn(NO_3)_2{\cdot}6H_2O$ (10 mmol) and 2-methylimidazole (80 mmol) were separately dissolved in 50 mL of methanol, and then both were quickly mixed. The mixture was stirred at 200 rpm for 24 h at room temperature. The obtained, white-colored slurry was collected by centrifugation at 10,000 rpm and washed with methanol three times, followed by drying in an oven at 60 C for overnight. For the synthesis of ZIF-8 derived heterostructure, the dried ZIP-8 was calcined in a controlled nitrogen environment at 700 C for 4 h.

2.3 Synthesis of pure Ag nanoparticles

Initially, 20 mL of distilled water was used to dissolve 2.2 mmol of $AgNO_3$. The solution was then continuously stirred at 200 rpm

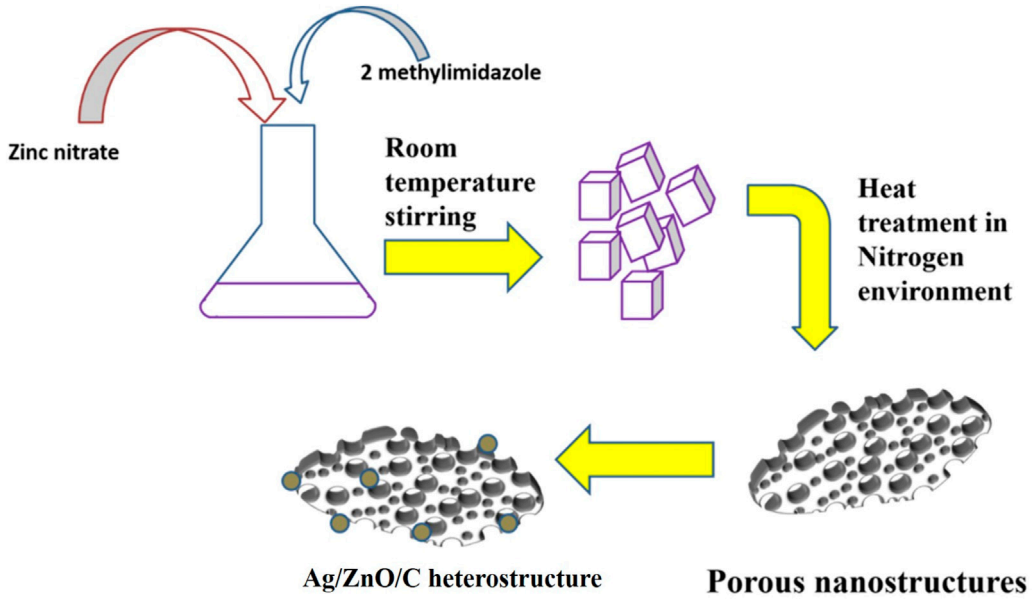

SCHEME 1
Synthesis scheme of the Ag/ZnO/C heterostructured photocatalyst.

while 2.5 mmol of $NaBH_4$ was added. The $NaBH_4$ was used as a reducing agent. To prevent any uncontrolled reduction of metal precursors, the solution was left in the dark for 1 hour. The solution turned grey after an hour, then the solution was centrifuged, and Ag nanoparticles were collected and dried.

2.4 Synthesis of photocatalyst

2.2 mmol of $AgNO_3$ was dissolved in 20 mL of distilled water containing 1 gm of synthesized ZnO sample. Subsequently, 2.5 mmol of $NaBH_4$ was mixed in the solution under continuous stirring. The $NaBH_4$ solution was used to reduce the Ag^+ precursor into its Ag^0 form. The solution was kept in the dark for 1 h. After 1 h, the solution turned grey (light or dark grey depending on the amount of silver content). Later, the solution was centrifuged, washed, and the samples were collected. Finally, the sample was dried at 60°C. The different variation of the photocatalysts was synthesized following the same procedure except varying the amount of silver content as 0.1%, 0.5%, 1%, and 1.5%. The resultant products were named Ag0.1/ZnO/C, Ag0.5/ZnO/C, Ag/ZnO/C, and Ag1.5/ZnO/C; respectively.

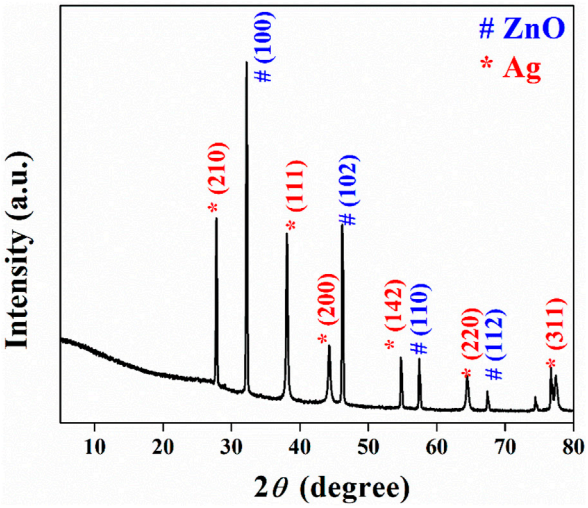

FIGURE 1
Detailed XRD spectra of Ag/ZnO/C sample.

2.5 Characterization of the synthesized sample

The synthesized samples were analyzed by different characterization techniques. A SmartLab, Rigaku (Japan) diffractometer was used to obtain XRD spectra from 5° to 90° using Cu K radiation. Field emission scanning electron microscopy (FESEM) and energy dispersive spectrometer (EDS) (Jeol JSM-7800F, Japan) used to study the morphology of the nanostructures. Jeol JEM-2100F (Japan) high-resolution transmission electron microscopy (TEM) was used to analyze the morphology and lattice structures. Moreover, the Renishaw Raman spectrometric analyzer (United Kingdom) using an Ar^+ ion laser with a 2.5 mW laser intensity was utilized to record the room temperature Raman spectra (excitation source with 514.5 nm line). The Raman spectra have a resolution of 0.5 cm^{-1}. Additionally, X-ray Photoelectron Spectroscopy (XPS) measurements were taken using the PHI 5000 Versa Probe III (Japan). At room temperature, a UV-Vis spectrometer (Shimadzu UV-2600, Japan) was used to calculate the photocatalytic removal of antibiotics in the region of 200–700 nm.

2.6 Assessment of photocatalytic activity

The photocatalytic degradation of Ciprofloxacin (CIP) under visible light irradiation was used to assess the photocatalytic activity of the samples as they were produced. A 200 W Xenon lamp was used as the light source and a 15 cm distance was kept between the light and the reactor. In a typical experiment, a 40 mg photocatalyst was added to 50 mL CIP solution (70 mg L^{-1}). The suspension was then magnetically stirred for 30 min in the dark to reach the adsorption-desorption equilibrium and then exposed to visible light. The aliquots were collected at scheduled time intervals, and the supernatant was separated by centrifugation. A further analysis was done for an aliquot solution by UV–Vis spectrophotometer. However, for the scavenger study, 1 mM of external agents such as IPA, AO, BQ, and silver nitrate was added to the original solution before photocatalysis.

3 Results and discussion

3.1 Synthesis and characterization of photocatalyst

The photocatalyst was developed by a simple precipitation method followed by annealing. Precursors were stirred at room temperature overnight to initiate the crystallization of ZIF-8. Zn^{+2} ions interact with the organic linker 2-methylimidazole as it diffuses into the system. Hence, the color of the solution turned turbid white, which makes it possible for the nucleation of ZIF-8 crystals. However, during pyrolysis, the polyhedral framework collapses, which yields homogeneous porous structures. The synthesis procedure was described in Scheme 1.

XRD analysis (Figure 1) was done to determine the crystallinity, phase, and composition of the synthesized samples. The detailed

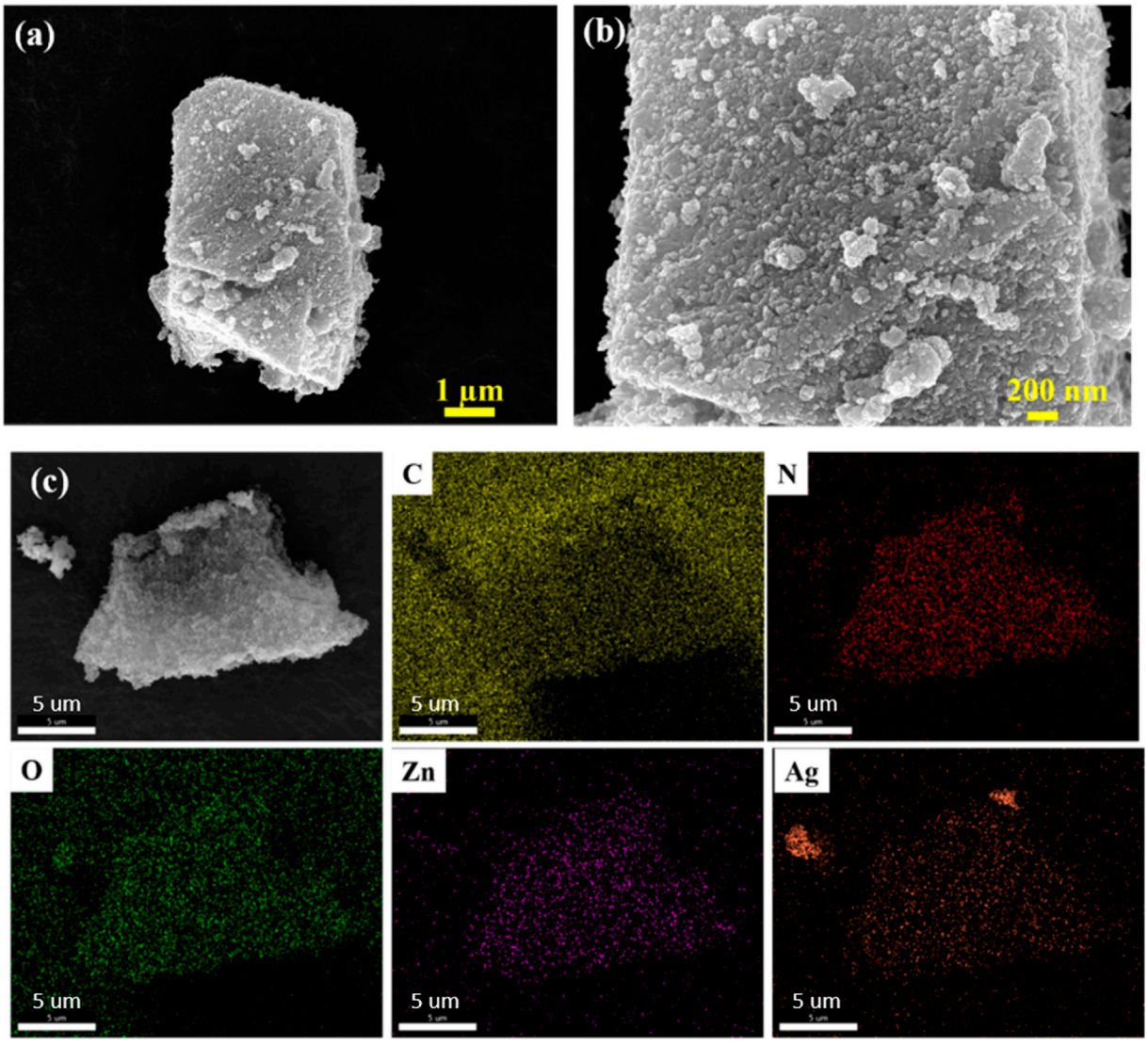

FIGURE 2
(a, b) FESEM images of Ag/ZnO/C photocatalyst **(c)** elemental mapping of individual atoms in Ag/ZnO/C.

XRD spectra of pristine ZnO (Supplementary Figure S1), Ag nanoparticles (Supplementary Figure S2) ZIF-8 crystal (Supplementary Figure S3) were provided in the supporting information. There were eight diffraction peaks eight diffraction peaks demonstrating the formation of wurtzite ZnO by calcining ZIF-8 (JCPDS, File No. 036–1,451). The incorporation of Ag nanoparticles imposes no shift in the ZnO characteristics peaks suggesting no alteration in the crystal structure of ZnO. The peaks at 38.24°, 44.19°, and 77.20° correspond to the (111), (200) and (311) planes of fcc silver nanoparticles (JCPDS, file No. 04–0,783). There were no peaks observed belonging to silver oxide (Meng, 2015; Wang S. et al., 2020).

The morphology of the heterostructure and the pristine ZIF-8 MOFs were evaluated using FESEM and HRTEM images (Figure 2). An excellent polyhedron structure with sharp edges was revealed by the FESEM images of pristine ZIF-8 (Supplementary Figure S4). The approximate size of the sides of a polyhedron was about 750 nm-1.5 μm. After carbonization, the ZIF-8 crystal transforms into a porous carbon network and ZnO. However, for the synthesis, no external carbon source was added in the synthesis method. The *ex-situ* attachment process of silver nanoparticles on the structures results in a uniform distribution of Ag nanoparticles throughout the structures (Supplementary Figure S5). The uniform distribution of metal nanoparticles was further confirmed by the Energy-dispersive X-ray spectroscopy (EDS) elemental mapping (Figure 2c).

TEM analysis was performed to further explore the morphology of Ag/ZnO/C heterostructure samples (Figure 3). The samples possess sheet-like morphology with well-distributed silver nanoparticles adhering to the surface. A lattice spacing of 0.24 nm corresponds to the (101) plane of hexagonal ZnO (Pramanik et al., 2023), while the 0.31 nm d spacing is attributed to the (111) plane of metallic Ag (Guo et al., 2024). This indicated that the Ag ions in the pores of the ZIF-8-derived structure were further reduced to the Ag^0 metallic state after the addition of the

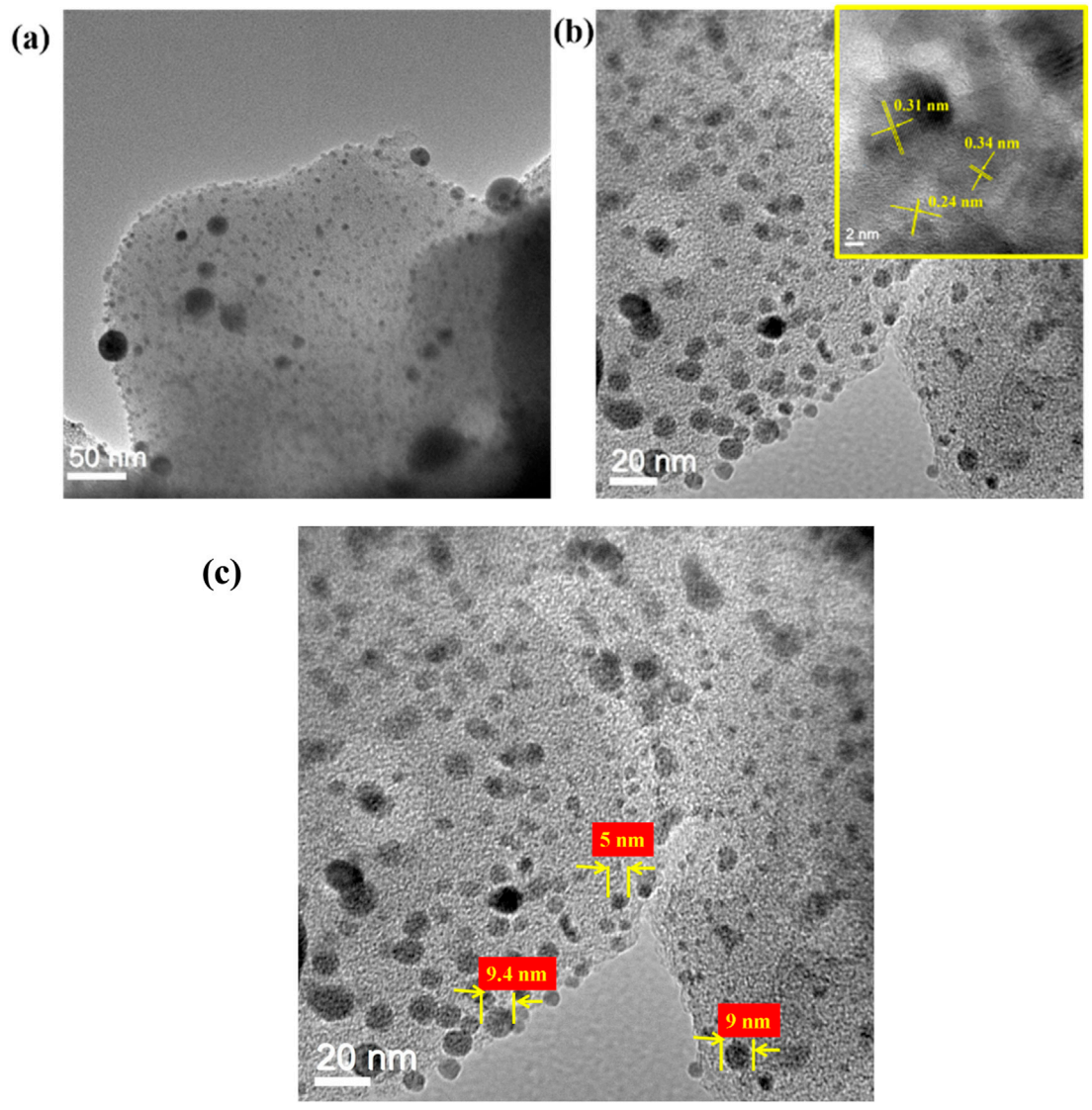

FIGURE 3
(a–c): TEM image of the Ag/ZnO/C with lattice image in the inset, and size distribution of nanoparticles.

$NaBH_4$ reductant. Additionally, the d spacing of 0.34 nm is ascribed to graphitic carbon present in the sample (Zhao and Zhang, 2021).

The elemental valence states of photocatalysts were studied using XPS survey spectra depicting the presence of intense peaks corresponding to Zn 2p, Ag 3d, C1s, and O 1s XPS, respectively (Figure 4). Two distinct peaks at around 284.8 and 287.6 eV that were attributed to the C-C and C=O bonds, respectively, may be seen in the high-resolution C 1s spectra (Wang et al., 2014). Two doublet peaks could be fitted in the Ag 3d spectra. The two peaks at 367.4 eV and 373.3 eV ascribe to Ag $3d_{5/2}$ and Ag $3d_{3/2}$ (Gu et al., 2020). The spin energy of the two above-mentioned peaks varied by ~6.0 eV, suggesting that Ag NPs within the photocatalyst structure existed in a zero-valence state (Gu et al., 2020). The XPS analysis of the oxygen reveals the presence of abundant oxygen defects in the heterostructure (Jain et al., 2019). There were two distinctive XPS peaks in Zn 2p spectra corresponding to $Zn2p_{1/2}$ and Zn $2p_{3/2}$, respectively (Song et al., 2014).

The two signature peaks at 1,322 and 1,572 cm^{-1} in Raman spectra correspond to the characteristics D and G bands of graphitic-like carbon. The formation of a graphitic layer of carbon is indicated by the G band, resulting from the first-order scattering effect of E_{2g} phonon sp^2 carbon atom. Moreover, the breathing mode of point

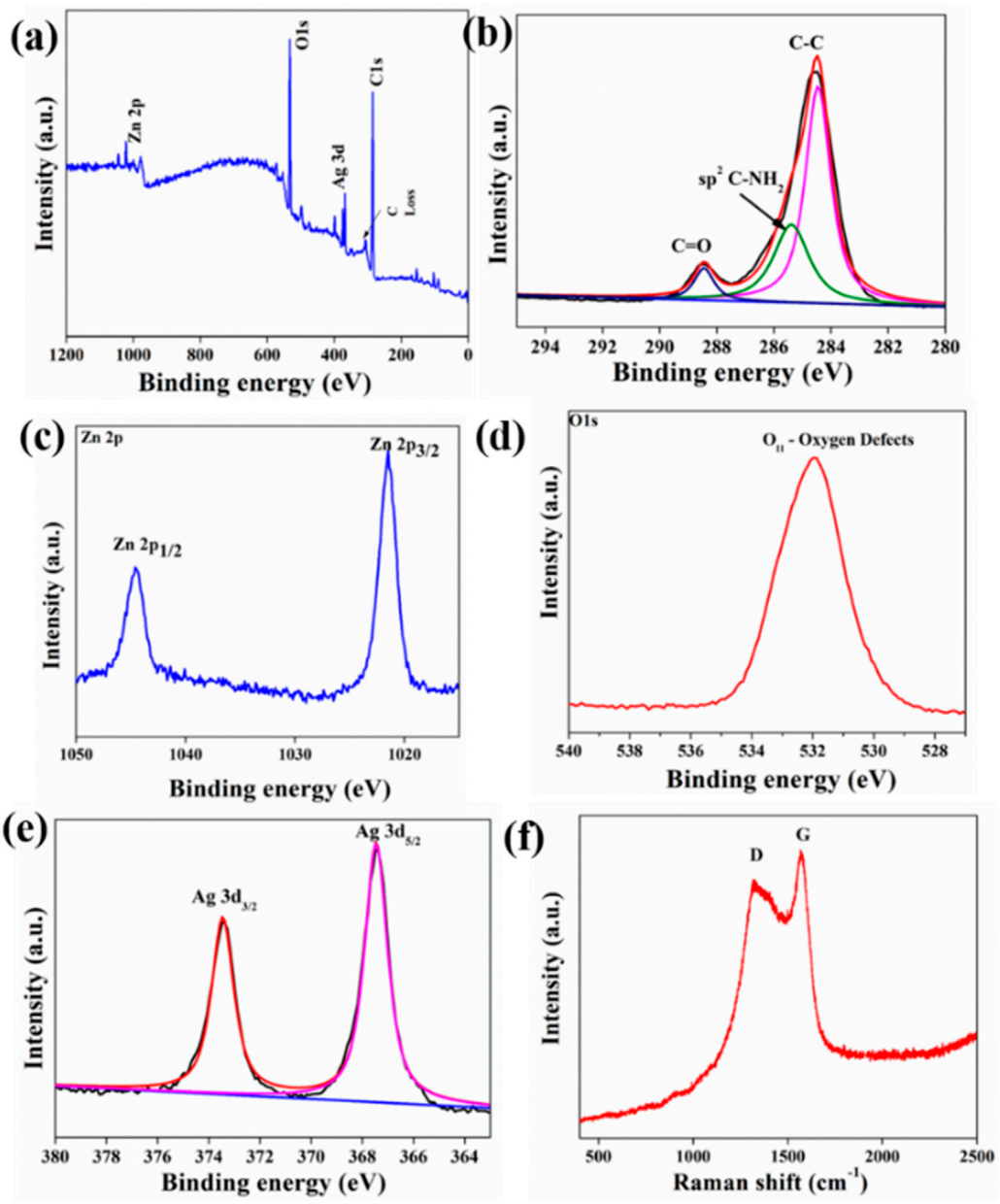

9

FIGURE 4
X-ray photoelectron spectroscopy (XPS) spectra of Ag/ZnO/C **(a)** survey spectra, **(b)** C1s spectra, **(c)** Zn2p spectra, **(d)** O1s spectra, and **(e)** Ag3d spectra **(f)** micro-Raman spectra of Ag/ZnO/C.

phonons with A_{1g} symmetry was described by the D band in Raman spectra. The well-developed layered-like graphitic structures were further supported by HRTEM images and band intensity ratio value (I_G/I_D = 0.90) (Figure 4). Similar results have also been reported in some recent studies (Young et al., 2016; Calderon et al., 2018; Masibi et al., 2022).

Brunauer-Emmett-Teller (BET) surface area analysis is done to give an isotherm model that involves the adsorption of gas over a certain range of pressure (Ahmad et al., 2024; Althabaiti et al., 2023). The surface area of the synthetic photocatalyst in this study was investigated using the nitrogen adsorption and desorption isotherms shown in Figures 5a-c. The sample possessed a surface area of 243.05 m^2g^{-1}. Furthermore, a mean pore diameter of 2.67 nm was shown by BET analysis. This analysis showed similarity to a type-III isotherm as per the IUPAC classification (Alghamdi et al., 2022).

3.2 Photocatalysis experiment against ciprofloxacin

The visible light photodegradation of CIP by synthesized photocatalysts was studied in laboratory conditions. A negligible amount of degradation was observed without any photocatalysts due to the inherent ability of the organic molecules to absorb light. The photoactivity of bare ZnO and silver nanoparticles was also low compared to the heterostructure photocatalyst Ag/ZnO/C (Supplementary Figure S6). We have also conducted the adsorption test for the sample in the dark. However, there is no signified removal by adsorption. After being exposed to visible light for 60 min, CIP degradation for the Ag/ZnO/C material was almost 98.11%. The improvement in photocatalytic activity for the heterostructure correlated to the enhanced light harvesting and high surface area derived from metal-organic frameworks. Additionally, the carbon and Ag act as electron sinks thus reducing the recombination rate of photo-induced carriers (Tran et al., 2019). However, pseudo-first-order kinetics were used to analyze the kinetic reaction rate of the photocatalytic reaction. As displayed in Supplementary Figure S8, the graph displayed a good linear correlation. In the graph, C_0 and C_t represent the concentration of antibiotics initially and after a certain time, respectively. The apparent pseudo-first-order rate constant (k) was estimated by the slope of ln (Ct/C_0) and time. Supplementary Figure S8 shows the apparent pseudo-first-order rate constants k = 58.04×10^{-3} min^{-1} for linear correlation in CIP removal by Ag/ZnO/C.

The heat-treated ZIF-8 samples were incorporated with different amounts of silver content. Among different loading samples, Ag/ZnO/C exhibits the fastest degradation which indicates the pivotal role of Ag nanoparticles in promoting effective electron transfer and reduction of recombination rate eventually leading to more effective degradation (Ng et al., 2016). On the contrary for the Ag 1.5/ZnO/C sample, a high amount of Ag loading depicts slower degradation probably caused by the agglomeration of Ag nanoparticles thus hindering the heterostructure surface from light radiation (Tran et al., 2019). The optimal amount of Ag was found to be 1 wt% based on the above results.

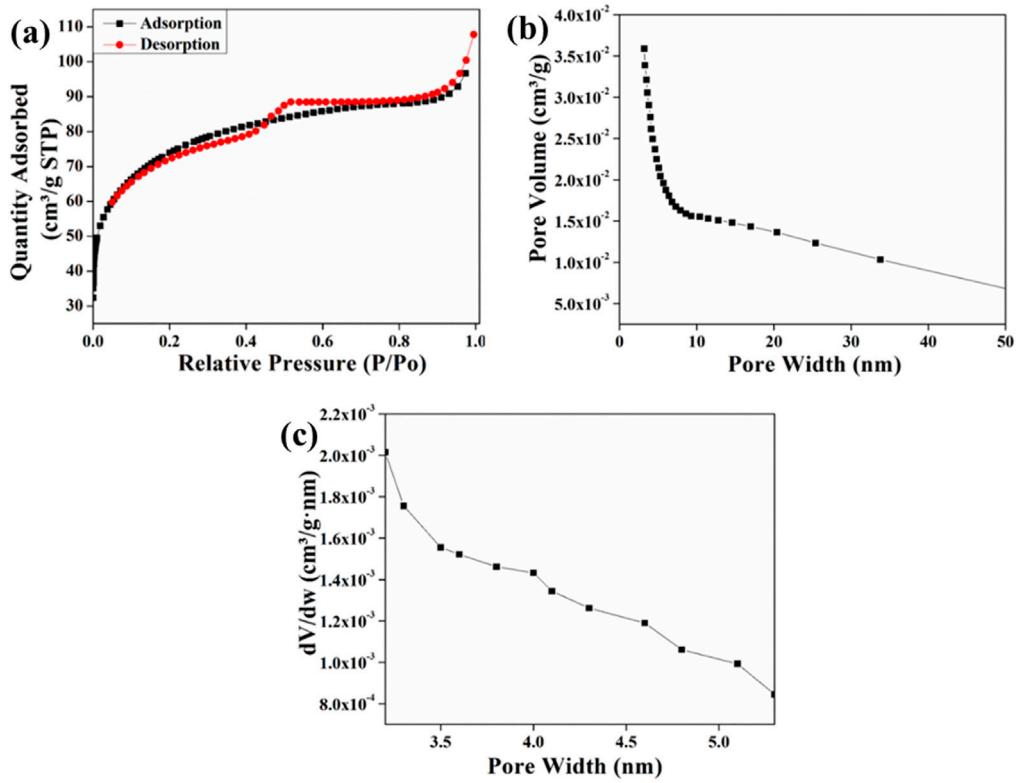

FIGURE 5
Brunauer-Emmett-Teller (BET) surface area analysis of Ag/ZnO/C heterostructure **(a)** N_2 adsorption/desorption isotherms, **(b)** pore volume vs. pore width **(c)** pore size distribution.

The effect of the amount of photocatalyst on the photocatalytic removal efficiency of CIP in aqueous solution was explored. We have considered different amounts of photocatalyst i.e., 10, 20, 30, 40, and 80 mg, respectively in 50 mL of antibiotic solution. It can be deduced that 40 mg of photocatalyst was needed to achieve optimum degradation of contaminants. The increase in dosage of photocatalyst from 40 mg to 80 mg results in a certain decrease in decomposition efficiency (Figure 6). Increased photocatalyst loading enhanced the accessible surface of the catalyst, which in turn led to an escalation in the reactive sites for the production of active radicals like hydroxyl and superoxide. However, the application of catalyst dosage above optimized concentration results reduction in removal efficiency, owing to the increase in light scattering effect and solution turbidity in the aqueous solution inhibiting the transition of visible light irradiation through the solution (Nosrati et al., 2012).

An essential component of the research was the investigation of the effect of initial antibiotic concentration on photocatalytic degradation. The initial antibiotic concentration was varied after keeping all the other reaction parameters constant. The photocatalytic degradation behavior (Figure 5) can be explained by the fact that, as the initial antibiotic loading increases, the active sites for producing reactive radicals remain constant while the catalyst concentration and light irradiation intensity both stable (Dimitrakopoulou et al., 2012).

Reusability was a very important aspect of a photocatalyst hence recycling reactions were performed for the photodegradation of CIP under visible light irradiation. The photocatalyst was collected by centrifugation followed by washing and reused the same for photodegradation keeping other reaction parameters constant. The time course of antibiotic degradation during four consecutive cycles under visible light was demonstrated in Figure 7. No subsequent changes in the photocatalytic activity have been observed after the fourth cycle indicating excellent stability for the photocatalyst material. Additionally, the XRD analysis (Supplementary Figure S7) of the sample before and after the photocatalysis indicated maintained structural integrity and no structural transformation after the photocatalysis process.

3.3 Photocatalytic mechanism

A plausible photocatalytic mechanism was explored based on the scavenger experiment to estimate the reactive active species generation. Figure 6b shows that the modification in the photocatalytic degradation of antibiotics by Ag/ZnO/C with the addition of ammonium oxalate (AO) (a quencher of h^+), benzoquinone (BQ) (a quencher of $O_2 \cdot^-$) and isopropanol (IPA) (a quencher of ·OH), silver nitrate (a quencher of e^-), respectively. 1 mM of external agents such as IPA, AO, BQ, and silver nitrate was added to the original solution before photocatalysis. It was explored that the degradation efficiency was greatly decreased by the addition of AO and BQ, respectively. On the contrary, other quenchers do not

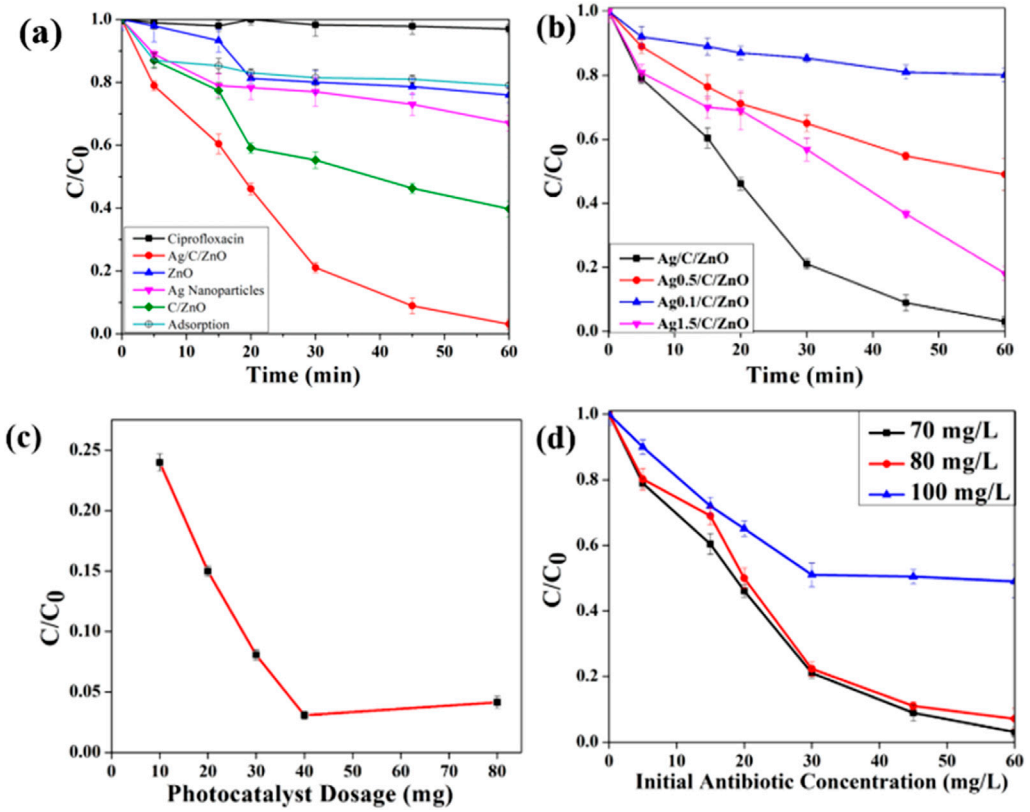

FIGURE 6
(a) Effect of contact time on degradation efficiency for initial concentration of CIP (70 ppm) **(b)** Effect of Ag loading on the photocatalytic degradation efficiency **(c)** Effect of photocatalyst dosage **(d)** Effect of initial concentration.

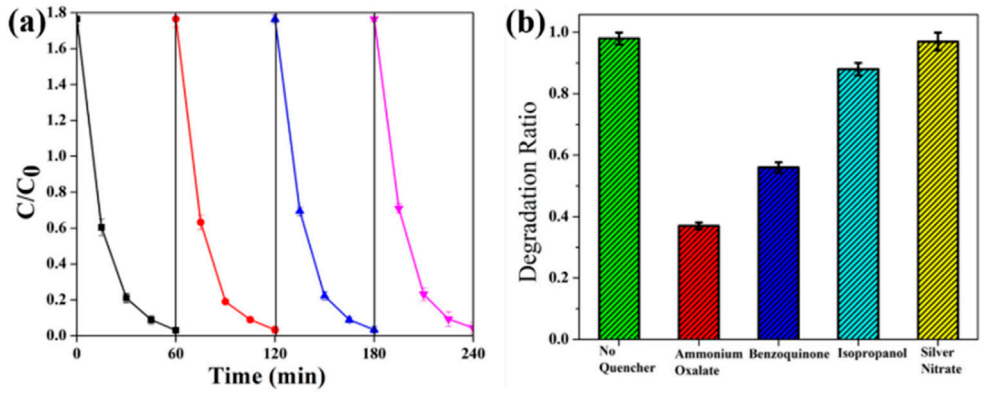

FIGURE 7
(a) Reusability studies of the photocatalyst **(b)** Trapping experiment of reactive active species during the photocatalysis of antibiotics under visible light irradiation.

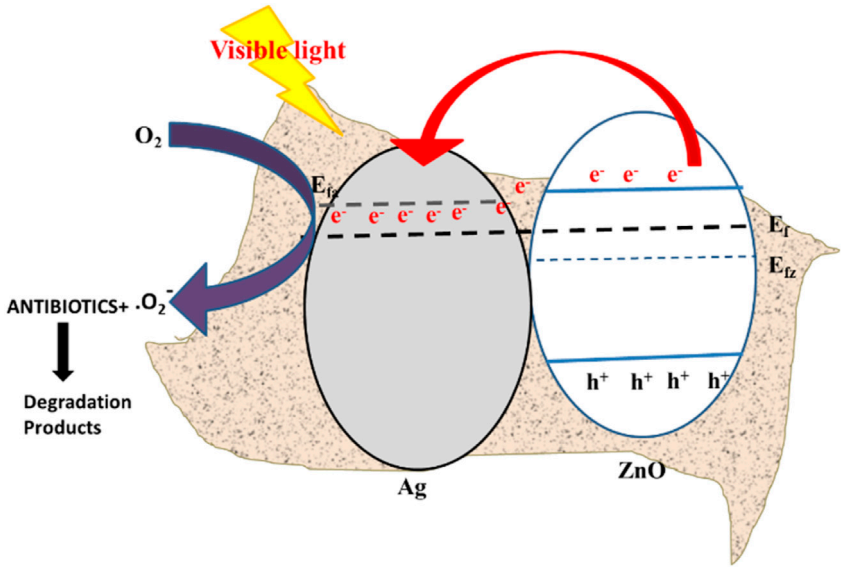

SCHEME 2
Schematic of the proposed energy-band structure of electron transfer for the Ag/ZnO/C heterostructure interface.

TABLE 1 Table of comparison of photocatalytic activities against ciprofloxacin by MOF-related heterostructure.

Photocatalyst	Removal efficiency (%)	Equilibrium time (h)	Light medium	Generated ROS	References
$ZnFe_2O_4$(ZFO)@RGO	73.4	1	Solar light	$\cdot O_2$–	Behera et al. (2019)
ZFCN@20PPY	92	2	Visible light	$\cdot O_2$–	Das et al. (2020)
Ag_2CrO_4/Ag/ $BiFeO_3$@RGO	96	1	Visible light	·OH and $\cdot O_2^-$	Kumar et al. (2019)
$NaYF_4$:Yb,Tm@TiO_2	97	2	Solar light	—	Ma and Li, (2019)
$CuFe_2O_4$@MC	80.77	1.5	UV	—	Tamaddon et al. (2020)
MOF mediated Ag/ZnO/C	**98.11**	**1**	**Visible**	h^+ and $\cdot O_2^-$	**This work**

Bold values indicate the finding of current studies.

affect the degradation efficiency of the photocatalysis process. The above result inferred that the photocatalytic mechanism was mainly dominated by generated h^+ and $\cdot O_2^-$(Liu et al., 2017). The Ag nanoparticles decorated on the ZIF-8-derived C/ZnO nanostructure act as an efficient visible light absorber due to the LSPR effect. The visible light harnessing could be supported by the bandgap ($E_{g,}$ ~1.8 eV) calculated by Tauc's plot from UV-Vis data (Supplementary Figure S9) for the heterostructure. There was a noticeable shift in bandgap with the pristine MOF ($E_{g,}$ ~2.8 eV) after the incorporation of silver nanoparticles due to electron transfer between them (Scheme 2). The reaction pathway was described by the given equation:

$$Ag + hv \rightarrow Ag\,(e^-) + Ag\,(h^+) \quad (1)$$

$$h^+ + H_2O \rightarrow H^+ + \cdot OH \quad (2)$$

$$Ag\,(e^-) + O_2 \rightarrow Ag\,(O_2\cdot^-) \quad (3)$$

$$Ag\,(O_2\cdot^-) + \text{Antibiotics} \rightarrow \text{Degradation product} \quad (4)$$

$$\cdot OH + \text{Antibiotics} \rightarrow \text{Degradation product} \quad (5)$$

The high reactivity of $O_2\cdot^-$ influences the diffusion in the bulk solution was quite difficult thus only the adsorbed antibiotics on the photocatalyst surface can be degraded. Subsequently, the strong adsorption capacity of ZIF-8 derived heterostructure eases the transportation of antibiotic molecules efficiently and promotes the utilization of h^+ and $\cdot O_2^-$. for photodegradation. Lastly, the unique topology of MOF-derived structures provides a large surface area for the silver nanoparticles restricting them from agglomeration. As silver nanoparticles were encapsulated in the pore opening of the MOF-derived structures, the surface of Ag/ZnO/C promotes the eradication of ciprofloxacin to a great extent. Similar reports were also found in the photocatalytic degradation of Congo red (CR) with zinc oxide coupled cadmium tungstate (ZnO-CT) (Fatima et al., 2023). Overall, this research will contribute to developing an efficient photocatalyst for practical water treatment.

4 Conclusion

In this study, as prospective visible light responsive photocatalysts, we synthesized the Ag decorated MOF derived heterostructure (Ag/ZnO/C) utilizing an easy wet chemical approach. The successful formation of a graphitic layer of carbon after the carbonization of ZIF-8 was indicated by the presence of D and G bands in the Raman spectra. The XRD and XPS spectra indicated the presence of only Ag^0 in the system. Furthermore, XPS studies highlighted the presence of abundant oxygen defects in the structure. At optimum conditions, the photocatalyst achieved 98% degradation efficiency in only 60 min of visible light irradiation with a rate constant of 58.04×10^{-3} min^{-1}. It has been demonstrated that the synergistic effect of metal nanoparticles and ZIF-8-derived structure increased the degradation of ciprofloxacin when exposed to visible light. The heterostructure demonstrated improved removal efficiency for antibiotics as compared to the pure ZIF-8. The excellent efficiency can be correlated to the good surface area of 243.05 m^2g^{-1}. The generation and dominating effect of h^+ and $\cdot O_2^-$ was indicated by the scavenger experiment in the photocatalytic process. As silver nanoparticles were encapsulated in the pore opening of the ZIF-8-derived structures, the surface of Ag/ZnO/C promotes the eradication of ciprofloxacin to a great extent. The resultant material has shown good reusability, for around 4 cycles without any discernible changes in the efficiency due to the encapsulation of Ag NPs. These results when compared with earlier studies (Table 1), indicated that the MOF-mediated heterostructure can be a viable and efficient photocatalyst in terms of water treatment in the future. So we believe that there is a need for further investigation of the catalytic activity of this photocatalyst for removing other antibiotics in real samples.

Data availability statement

The original contributions presented in the study are included in the article/Supplementary Material, further inquiries can be directed to the corresponding authors.

Author contributions

PB: Methodology, Writing–original draft, Writing–review and editing. RP: Conceptualization, Supervision, Visualization, Writing–original draft, Writing–review and editing. SC: Conceptualization, Funding acquisition, Validation, Visualization, Writing–original draft, Writing–review and editing.

Funding

The author(s) declare that financial support was received for the research, authorship, and/or publication of this article. PB and SC acknowledge UGC-DAE-CSR for their funding support.

Conflict of interest

The authors declare that the research was conducted in the absence of any commercial or financial relationships that could be construed as a potential conflict of interest.

Publisher's note

Supplementary material

The Supplementary Material for this article can be found online at: https://www.frontiersin.org/articles/10.3389/fnano.2025.1477247/full#supplementary-material

References

Ahmad, R., Alzahrani, E. A., Dwivedi, P., Hafeez, S., Deswal, J., Fatima, B., et al. (2024). Biodegradable acid-based Fe2MnO4 nanoparticles for water remediation. *Molecules* 29, 3867. doi:10.3390/molecules29163867

Alghamdi, Y. G., Krishnakumar, B., Malik, M. A., and Alhayyani, S. (2022). Design and preparation of biomass-derived activated carbon loaded TiO2 photocatalyst for photocatalytic degradation of reactive red 120 and ofloxacin. *Polymers* 14, 880. doi:10.3390/polym14050880

Althabaiti, S. A., Khan, Z., Malik, M. A., Bawaked, S. M., Al-Sheheri, S. Z., Mokhtar, M., et al. (2023). Biomass-derived carbon deposited TiO 2 nanotube photocatalysts for enhanced hydrogen production. *Nanoscale Adv.* 5, 3671–3683. doi:10.1039/d3na00211j

Assar, S., Nosratabadi, R., Khorramdel Azad, H., Masoumi, J., Mohamadi, M., and Hassanshahi, G. (2021). A review of immunomodulatory effects of fluoroquinolones. *Immunol. Investig.* 50 (8), 1007–1026. doi:10.1080/08820139.2020.1797778

Basak, S., Bhattacharyya, P., Pudake, R. N., Lokhande, P. E., Rednam, U., and Chakrabarti, S. (2024). Metal-organic framework as nanocarriers for agricultural applications: a review. *Front. Nanotechnol.* 6, 1385981. doi:10.3389/fnano.2024.1385981

Behera, A., Kandi, D., Mansingh, S., Martha, S., and Parida, K. (2019). Facile synthesis of ZnFe2O4@ RGO nanocomposites towards photocatalytic ciprofloxacin degradation and H2 energy production. *J. Colloid Interface Sci.* 556, 667–679. doi:10.1016/j.jcis.2019.08.109

Bergaoui, M., Khalfaoui, M., Awadallah-F, A., and Al-Muhtaseb, S. (2021). A review of the features and applications of ZIF-8 and its derivatives for separating CO2 and isomers of C3-and C4-hydrocarbons. *J. Nat. Gas Sci. Eng.* 96, 104289. doi:10.1016/j.jngse.2021.104289

Bhatt, S., and Chatterjee, S. (2022). Fluoroquinolone antibiotics: occurrence, mode of action, resistance, environmental detection, and remediation–A comprehensive review. *Environ. Pollut.* 315, 120440. doi:10.1016/j.envpol.2022.120440

Bhattacharyya, P., Basak, S., and Chakrabarti, S. (2021). Advancement towards antibiotic remediation: heterostructure and composite materials. *Chemistryselect* 6 (29), 7323–7345. doi:10.1002/slct.202100436

Calderon, N. Z., Ampuero, J. L., La Rosa-Toro, A., and and Pujada, B. R. (2018). "Influence of substrate temperature on the properties of Ag-C films produced by DC Magnetron Sputtering," in *Journal of physics: conference series*. Lima, Peru: IOP Publishing.

Chen, C., Fei, L., Wang, B., Xu, J., Li, B., Shen, L., et al. (2024). MOF-based photocatalytic membrane for water purification: a review. *Small* 20, 2305066. doi:10.1002/smll.202305066

Dai, H., Yuan, X., Jiang, L., Wang, H., Zhang, J., Zhang, J., et al. (2021). Recent advances on ZIF-8 composites for adsorption and photocatalytic wastewater pollutant removal: fabrication, applications and perspective. *Coord. Chem. Rev.* 441, 213985. doi:10.1016/j.ccr.2021.213985

Das, K. K., Patnaik, S., Mansingh, S., Behera, A., Mohanty, A., Acharya, C., et al. (2020). Enhanced photocatalytic activities of polypyrrole sensitized zinc ferrite/graphitic carbon nitride nn heterojunction towards ciprofloxacin degradation, hydrogen evolution and antibacterial studies. *J. Colloid Interface Sci.* 561, 551–567. doi:10.1016/j.jcis.2019.11.030

Dimitrakopoulou, D., Rethemiotaki, I., Frontistis, Z., Xekoukoulotakis, N. P., Venieri, D., and Mantzavinos, D. (2012). Degradation, mineralization and antibiotic inactivation of amoxicillin by UV-A/TiO2 photocatalysis. *J. Environ. Manag.* 98, 168–174. doi:10.1016/j.jenvman.2012.01.010

Elhalil, A., Elmoubarki, R., Farnane, M., Machrouhi, A., Mahjoubi, F., Sadiq, M., et al. (2019). Novel Ag-ZnO-La2O2CO3 photocatalysts derived from the Layered Double Hydroxide structure with excellent photocatalytic performance for the degradation of pharmaceutical compounds. *J. Sci. Adv. Mater. Devices* 4 (1), 34–46. doi:10.1016/j.jsamd.2019.01.002

Fatima, B., Siddiqui, S., Ahmed, R., and Chaudhry, S. A. (2019). Preparation of functionalized CuO nanoparticles using Brassica rapa leave extract for water purification. *Desalin. Water Treat.* 164, 192–205. doi:10.5004/dwt.2019.24393

Fatima, B., Siddiqui, S. I., Rajor, H. K., Malik, M. A., Narasimharao, K., Ahmad, R., et al. (2023). Photocatalytic removal of organic dye using green synthesized zinc oxide coupled cadmium tungstate nanocomposite under natural solar light irradiation. *Environ. Res.* 216, 114534. doi:10.1016/j.envres.2022.114534

Gangar, T., and Patra, S. (2023). Antibiotic persistence and its impact on the environment. *3 Biotech.* 13 (12), 401. doi:10.1007/s13205-023-03806-6

Gu, A., Chen, J., Gao, Q., Khan, M. M., Wang, P., Jiao, Y., et al. (2020). The preparation of Ag/ZIF-8@ ZIF-67 core-shell composites as excellent catalyst for degradation of the nitroaromatic compounds. *Appl. Surf. Sci.* 516, 146160. doi:10.1016/j.apsusc.2020.146160

Guo, X., Dong, C., Gao, M., Ye, D., Dai, Q., Zhan, W., et al. (2024). Crystal-facet-dependent activity and N2 yield of Ag/CeO2 catalysts for catalytic oxidation of N, N-Dimethylformamide. *Appl. Catal. B Environ.* 341, 123286. doi:10.1016/j.apcatb.2023.123286

Hayri-Senel, T., Kahraman, E., Sezer, S., Erdol-Aydin, N., and Nasun-Saygili, G. (2024). Photocatalytic degradation of ciprofloxacin from water with waste polystyrene and TiO_2 composites. *Heliyon* 10 (3), e25433. doi:10.1016/j.heliyon.2024.e25433

Hussain, M. Z., Yang, Z., Huang, Z., Jia, Q., Zhu, Y., and Xia, Y. (2021). Recent advances in metal–organic frameworks derived nanocomposites for photocatalytic applications in energy and environment. *Adv. Sci.* 8 (14), 2100625. doi:10.1002/advs.202100625

Jain, S., Shah, J., Negi, N. S., Sharma, C., and Kotnala, R. K. (2019). Significance of interface barrier at electrode of hematite hydroelectric cell for generating empower by water splitting. *Int. J. Energy Res.* 43 (9), 4743–4755. doi:10.1002/er.4613

Kumar, A., Sharma, G., Naushad, M., Ahamad, T., Veses, R. C., and Stadler, F. J. (2019). Highly visible active Ag2CrO4/Ag/BiFeO3@ RGO nano-junction for photoreduction of CO2 and photocatalytic removal of ciprofloxacin and bromate ions: the triggering effect of Ag and RGO. *Chem. Eng. J.* 370, 148–165. doi:10.1016/j.cej.2019.03.196

Li, Y.-R., Dong, X., Pan, S.-Y., Luo, L., Lei, H.-T., and Xu, Z.-L. (2024). Design to enhance sensing performance of ZIF-8 crystals. *Prog. Nat. Sci. Mater. Int.* 34, 240–250. doi:10.1016/j.pnsc.2024.02.011

Liu, J., Li, R., Wang, Y., Wang, Y., Zhang, X., and Fan, C. (2017). The active roles of ZIF-8 on the enhanced visible photocatalytic activity of Ag/AgCl: generation of superoxide radical and adsorption. *J. Alloys Compd.* 693, 543–549. doi:10.1016/j.jallcom.2016.09.201

Liu, Y., Cheng, H., Cheng, M., Liu, Z., Huang, D., Zhang, G., et al. (2021). The application of Zeolitic imidazolate frameworks (ZIFs) and their derivatives based materials for photocatalytic hydrogen evolution and pollutants treatment. *Chem. Eng. J.* 417, 127914. doi:10.1016/j.cej.2020.127914

Ma, Y., and Li, S. (2019). NaYF 4: Yb, Tm@ TiO 2 core@ shell structures for optimal photocatalytic degradation of ciprofloxacin in the aquatic environment. *RSC Adv.* 9, 33519–33524. doi:10.1039/c9ra08145c

Masibi, E. G., Makhetha, T. A., and Moutloali, R. M. (2022). Effect of the incorporation of ZIF-8@ GO into the thin-film membrane on salt rejection and BSA fouling. *Membranes* 12 (4), 436. doi:10.3390/membranes12040436

Meng, Y. (2015). A sustainable approach to fabricating Ag nanoparticles/PVA hybrid nanofiber and its catalytic activity. *Nanomaterials* 5 (2), 1124–1135. doi:10.3390/nano5021124

Mishra, A., Kukreja, E. A., Pudake, R. N., Kumar, R., Singh, M. P., Yadav, L., et al. (2023). Label-free selective and sensitive colorimetric detection of ampicillin in milk and water using silver nanoparticles. *J. Food Compos. Analysis* 119, 105256. doi:10.1016/j.jfca.2023.105256

Ng, K. H., Lee, C. H., Khan, M. R., and Cheng, C. K. (2016). Photocatalytic degradation of recalcitrant POME waste by using silver doped titania: photokinetics and scavenging studies. *Chem. Eng. J.* 286, 282–290. doi:10.1016/j.cej.2015.10.072

Nosrati, R., Olad, A., and Maramifar, R. (2012). Degradation of ampicillin antibiotic in aqueous solution by ZnO/polyaniline nanocomposite as photocatalyst under sunlight irradiation. *Environ. Sci. Pollut. Res.* 19, 2291–2299. doi:10.1007/s11356-011-0736-5

Oh, S., Nguyen, H. T., Obayomi, K. S., and Siddiqui, S. I. (2024). Assessing the environmental risk potential of transformation byproducts formed during fungal enzymatic treatment of a pharmaceutical mixture. *J. Industrial Eng. Chem.* 142, 725–735. doi:10.1016/j.jiec.2024.08.015

Pettinari, C., Marchetti, F., Mosca, N., Tosi, G., and Drozdov, A. (2017). Application of metal– organic frameworks. *Polym. Int.* 66 (6), 731–744. doi:10.1002/pi.5315

Pramanik, S., Das, S., Karmakar, R., Irsad Ali, S., Mukherjee, S., Dey, S., et al. (2023). Enhancement of UV luminescence in Zn/ZnO nanocomposites synthesized by controlled thermal oxidation of Zn nano-octahedral. *J. Luminescence* 257, 119746. doi:10.1016/j.jlumin.2023.119746

Shariati, A., Arshadi, M., Khosrojerdi, M. A., Abedinzadeh, M., Ganjalishahi, M., Maleki, A., et al. (2022). The resistance mechanisms of bacteria against ciprofloxacin and new approaches for enhancing the efficacy of this antibiotic. *Front. public health* 10, 1025633. doi:10.3389/fpubh.2022.1025633

Song, K.-W., Park, M.-H., Kim, T.-H., Lim, S.-H., and Yang, C.-W. (2014). UV enhanced synthesis of high-density Au coated ZnO nanocomposite. *J. Nanosci. Nanotechnol.* 14 (11), 8766–8770. doi:10.1166/jnn.2014.10013

Tamaddon, F., Nasiri, A., and Yazdanpanah, G. (2020). Photocatalytic degradation of ciprofloxacin using CuFe2O4@ methyl cellulose based magnetic nanobiocomposite. *MethodsX* 7, 100764. doi:10.1016/j.mex.2019.12.005

Tran, M. L., Nguyen, C. H., Fu, C.-C., and Juang, R.-S. (2019). Hybridizing Ag-Doped ZnO nanoparticles with graphite as potential photocatalysts for enhanced removal of metronidazole antibiotic from water. *J. Environ. Manag.* 252, 109611. doi:10.1016/j.jenvman.2019.109611

Wang, C., Kim, J., Tang, J., Kim, M., Lim, H., Malgras, V., et al. (2020a). New strategies for novel MOF-derived carbon materials based on nanoarchitectures. *Chem* 6 (1), 19–40. doi:10.1016/j.chempr.2019.09.005

Wang, H.-T., Liu, Y.-P., Zhang, H., Chang, N., Shao, W., Shi, M.-S., et al. (2019). Design and synthesis of porous C–ZnO/TiO2@ZIF-8 multi-component nano-system via pyrolysis strategy with high adsorption capacity and visible light photocatalytic activity. *Microporous Mesoporous Mater.* 288, 109548. doi:10.1016/j.micromeso.2019.06.010

Wang, Q., Gao, Q., Al-Enizi, A. M., Nafady, A., and Ma, S. (2020b). Recent advances in MOF-based photocatalysis: environmental remediation under visible light. *Inorg. Chem. Front.* 7 (2), 300–339. doi:10.1039/c9qi01120j

Wang, S., Jia, F., Wang, X., Hu, L., Sun, Y., Yin, G., et al. (2020c). Fabrication of ZnO nanoparticles modified by uniformly dispersed Ag nanoparticles: enhancement of gas sensing performance. *ACS omega* 5 (10), 5209–5218. doi:10.1021/acsomega.9b04243

Wang, W., Chakrabarti, S., Chen, Z., Yan, Z., Tade, M. O., Zou, J., et al. (2014). A novel bottom-up solvothermal synthesis of carbon nanosheets. *J. Mater. Chem. A* 2 (7), 2390–2396. doi:10.1039/c3ta13593d

Xiao, W., Cheng, M., Liu, Y., Wang, J., Zhang, G., Wei, Z., et al. (2023). Functional metal/carbon composites derived from metal–organic frameworks: insight into structures, properties, performances, and mechanisms. *ACS Catal.* 13 (3), 1759–1790. doi:10.1021/acscatal.2c04807

Young, C., Salunkhe, R. R., Tang, J., Hu, C. C., Shahabuddin, M., Yanmaz, E., et al. (2016). Zeolitic imidazolate framework (ZIF-8) derived nanoporous carbon: the effect of carbonization temperature on the supercapacitor performance in an aqueous electrolyte. *Phys. Chem. Chem. Phys.* 18 (42), 29308–29315. doi:10.1039/c6cp05555a

Zhao, Y., and Zhang, X. (2021). *In situ* activation graphitization to fabricate hierarchical porous graphitic carbon for supercapacitor. *Sci. Rep.* 11 (1), 6825. doi:10.1038/s41598-021-85661-0